Cell and Substrate Temperatures of Glass/Glass and Glass/Polymer PV Modules

by

Balamurali Natarajan Rammohan

A Thesis Presented in Partial Fulfillment
of the Requirements for the Degree
Master of Science

Approved July 2017 by the
Graduate Supervisory Committee:

Govindasamy Tamizhmani, Chair
Devarajan Srinivasan
Joseph Kuitche

ARIZONA STATE UNIVERSITY

August 2017

ABSTRACT

Performance of photovoltaic (PV) modules decrease as the operating temperatures increase. In hot climatic conditions, the operating temperature can reach as high as 85°C for the rooftop modules. Considering a typical power drop of 0.5%/°C for crystalline silicon modules, a performance decrease of approximately 30% could be expected during peak summer seasons due to the difference between module rated temperature of 25°C and operating temperature of 85°C. Therefore, it is critical to accurately predict the temperature of the modules so the performance can be accurately predicted. The module operating temperature is based not only on the ambient and irradiance conditions but is also based on the thermal properties of module packaging materials. One of the key packaging materials that would influence the module operating temperature is the substrate, polymer backsheet or glass. In this study, the thermal influence of three different polymer backsheet substrates and one glass substrate has been investigated through five tasks:

1. Determination and modeling of substrate or module temperature of coupons using four different substrates (three backsheet materials and one glass material).
2. Determination and modeling of cell temperature of coupons using four different substrates (three backsheet materials and one glass material)
3. Determination of temperature difference between cell and individual substrates for coupons of all four substrates
4. Determination of NOCT (nominal operating cell temperature) of coupons using all four substrate materials
5. Comparison of operating temperature difference between backsheet substrate coupons.

All these five tasks have been executed using the specially constructed one-cell coupons with identical cells but with four different substrates. For redundancy, two coupons per substrate were constructed and investigated. This study has attempted to model the effect of thermal conductivity of backsheet material on the cell and backsheet temperatures.

To my father, mother and beloved sister

ACKNOWLEDGMENTS

First, I would like to thank my professor Dr. Govindasamy Tamizhmani for giving me this opportunity to work under him at the Photovoltaic Reliability Laboratory (PRL). His continuous support, constant encouragement and his valuable inputs irrespective of his busy schedule have been invaluable to my work. I would also like to thank Dr. Jaewon Oh for his valuable inputs and constant support throughout this project. I would also like to thank PRL's technical manager Mr. Sai Tatapudi and all my lab colleagues for helping me out with my experiments whenever I needed and requested for help. I would like to thank my thesis committee members Dr. Joseph Kuitche and Dr. Devarajan Srinivasan for showing interest in my work and extending their support. Special thanks to my friend and colleague Aravind Srinivasan who rendered his constant support throughout the analysis and modeling phase of the project. Finally, I would like to thank the lord almighty for making all this happen.

TABLE OF CONTENTS

Page

CHAPTER Page

CHAPTER Page

LIST OF TABLES

LIST OF FIGURES

Figure Page

Figure Page

Figure Page

1.0 INTRODUCTION

1.1 Background

Solar energy is one of the clean and renewable forms of energy with everlasting sun as its energy source. Though the increased environmental awareness among the public and corporates is one of the factors for increase in photovoltaic deployment worldwide, it can be mainly attributed to drastic fall in module and energy price for over the last two decades. Photovoltaics is now able to effectively compete with the other fossil fuel energy sources in the commercial market because a lot of research went into performance and reliability improvement of photovoltaic systems over the past few decades to make it economically viable. Hence it is very much important to understand the factors affecting the performance of PV modules in order for photovoltaics to survive and thrive in the competitive energy market.

Photovoltaic modules absorb the photons from the sunlight and convert them into electrons. Among all other PV technologies, crystalline silicon continues to be the market leader since the emergence of PV industry. The crystalline silicon module construction typically consists of glass as superstrate and backsheet polymers or glass as substrate. The performance of crystalline silicon modules is mainly affected by irradiance and operating temperature. Irradiance directly affects the current produced in the module while operating temperature primarily affects the voltage. In general, the voltage decreases by 1 % for every 2.5°C rise in temperature while the power decreases by 1 % for every 2.2°C rise in temperature.

In hot climatic regions like Arizona, the open rack modules typically operate at around 65°C during summer. Hence there would be at least 18 % drop in power in this case as the

nameplate power data are rated at standards test conditions (STC) of 25°C. Moreover, the increased operating temperature induce thermal stresses in the module and acts as stressor for several degradation and failure modes. Hence it can be noted that higher temperature operation leads to both performance and reliability issues.

The operating temperature of a PV module in a plant is indeed affected by irradiance, wind speed, wind direction and module construction with ambient temperature being the dominant factor. According to law of conservation of energy, there exists an equilibrium. The part of energy from the sunlight is converted into electrons while rest of them gets absorbed or reflected by the module materials. The solar heating in the cell and the energy absorbed by the module materials heat up the cell. There exists a thermal equilibrium between heat absorption, generation in the module and heat loss. Usually the heat loss happens in the form of conduction, convection and radiation, and is very much dependent upon the thermal and optical properties of the module materials. The conductive heat transfer takes place between module materials while convection takes place between module surfaces and the air surrounding it. Radiative heat transfer takes place between surface of the module and the sky and the ground.

The focus of this study is to determine the effect of ambient conditions and material properties of the substrate on operating cell and module temperature for modules located in hot and dry climatic regions like Arizona. This study also provides a relationship between thermal properties of the substrates and the operating cell temperature for open rack photovoltaic systems

1.2 Problem Statement

The main objective of this study is to analyze the variation of the difference between cell and substrate temperature for monocrystalline silicon modules with different substrates for varying ambient conditions. Thermal models have been generated to predict the effect of ambient conditions on substrate and the cell temperature. There are several thermal models available in the existing literature but most of them do not account for the thermal conductivity of the substrate. Hence one such thermal model for module temperature is formulated based on field data collected from open rack mounted single cell coupons of different substrates installed at Arizona State University – Photovoltaic Reliability Laboratory (ASU-PRL).

This study also involves NOCT and operating temperature computation and comparison for all test coupons.

1.3 Scope of the Work

- Selection of different substrates for fabrication based on detailed market and literature survey.
- Design and fabrication of single cell coupons with three different polymer backsheets and glass as substrate.
- Light soaking of the fabricated coupons for more than 10 sun hours in order to remove light induced degradation as per the standard IEC-61215-2.
- Characterization testing of fabricated coupons which includes light and dark I-V, electroluminescence imaging, infrared imaging and spectral reflectance testing after light soaking.

- Fabrication of open mounting rack which meets the dimension requirements of nominal operating cell temperature rack as per the standard IEC-61215-2.
- Installation of eight fabricated coupons comprising of two coupons each corresponding to four different substrates in the rack.
- Collection and monitoring the ambient condition data every 30 seconds from the weather station installed at ASU-PRL.
- Programming and installation of data acquisition system comprising of Campbell scientific datalogger CR1000 and AM 16/32 multiplexers for coupon data collection.
- Collection and monitoring of cell temperature and substrate temperature of all installed coupons.
- Time series analysis of difference between cell and substrate temperature for varying ambient conditions.
- Developing statistical models for prediction of cell and module temperature based on substrate properties and ambient conditions.
- Computing and comparing nominal operating cell temperatures for all installed coupons.

1.4 Limitations

Since the thermal model is based on data collected from single cell coupons, it might not be very accurate for big-sized module. It is because the temperature distribution in the single-cell coupon will be uniform throughout the coupon surface while it is not the case with the big-sized module wherein the temperature difference between cells near the center of the module and edge of the module is approximately around 2-4 °C. Also, the results

from the model might be applicable only for the crystalline silicon modules installed in hot-dry climatic regions like Arizona during summer months.

2.0 LITERATURE SURVEY

2.1 Temperature Influence on Photovoltaic Module Performance

There have been several studies which were performed in the past to evaluate the impact of operating temperature on the performance and reliability of photovoltaic modules. Skoplaki et al [1] presented various correlations showing linear dependence of both electrical efficiency and power output on operating temperature. Going into the physics of the problem, increase in temperature decreases band gap of the solar cell and lower energy photons tend to get absorbed leading to rapid decrease in open-circuit voltage and a slight increase in short-circuit current thereby causing drop in fill factor and efficiency [2]. Just like any other semiconductor device, solar cell is also sensitive to temperature changes [3].

The temperature coefficient is used to determine the effect of temperature on the output voltage, current or module power. The typical values of temperature coefficients of output power, voltage and current for crystalline silicon cells are -0.5%/°C, -0.4%/^{o}C and +0.06%/^{o}C, respectively [4].

2.2 Thermal Models

Since the temperature of a PV module is directly related to module power output, a lot of effort has gone into developing thermal models in the past. They were developed either through empirical approach based on field data or theoretical approach based on heat balance. Most of them illustrates the dependence of temperature on ambient conditions (irradiance, wind speed, and ambient temperature), module installation and the module configurations. A few of the popular and relevant thermal models have been reviewed in this section.

2.2.1 Simple Model

The simple model is applicable for calculating operating cell temperature for open rack mounting and low windspeed conditions [5]. This model is similar to a line equation with ambient temperature as intercept and it shows a direct proportional relation to irradiance.

$$T_{cell} = T_{ambient} + 0.031 \times Irradiance$$

Where,

T_{cell}: Cell Temperature (°C)

$T_{ambient}$: Ambient Temperature (°C)

$Irradiance$: Solar irradiance (W/m^2)

2.2.2 NOCT Model

Just like the previous model, this model is also applicable only in the case of open-rack mounting and low wind speed conditions. Using this model, the module temperature can be determined based on ambient temperature, irradiance and module's nominal operating cell temperature as follows [6].

$$T_{module} = T_{ambient} + (T_{NOCT} - 20) \times \frac{Irradiance}{800}$$

Where,

T_{module}: module Temperature (°C)

$T_{ambient}$: ambient temperature (°C)

T_{NOCT}: nominal operating cell temperature of the module (°C)

$Irradiance$: Solar irradiance (W/m^2)

2.2.3 IEC 61853 Model

The thermal model as per the standard IEC 61853 is applicable for a specific wind speed range [7].

$$T_{module} - T_{ambient} = b \times G + a$$

Where,

T_{module}: module Temperature (°C)

$T_{ambient}$: ambient temperature (°C)

a, b: coefficients for a certain wind speed range

G: Solar irradiance (W/m^2)

2.2.4 Tang's Model

Yingtang Tang's master thesis [8] illustrates a model for temperature prediction of a large photovoltaic module in an open-rack system with respect to ambient conditions. In total, three models were formulated by Tang in this thesis.

Tang's model is shown in the equation below.

$$T_{mod} = w_1 \times T_{amb} + w_2 \times E + w_3 \times Windspd + w_4 \times WindDir + w_5 \times Humidity + c$$

Where,

T_{mod}: module Temperature (°C)

$T_{ambient}$: ambient temperature (°C)

E: irradiance (W/m^2)

$Windspd$: wind speed (m/s)

$WindDir$: wind Direction (°)

$Humidity$: relative humidity

w_1, w_2, w_3, w_4, w_5 : coefficients

c : constant

The results from the model showed that the operating temperature was very much dependent upon the ambient temperature and also irradiance and wind speed to some extent. However, the effect of wind direction and relative humidity were almost negligible. So, a second model from his thesis without considering the effect of wind direction and relative humidity is shown below.

$$T_{mod} = w_1 \times T_{amb} + w_2 \times E + w_3 \times Windspd + c$$

Where,

T_{mod}: module Temperature (°C)

T_{amb}: ambient temperature (°C)

E: solar irradiance (W/m^2)

$Windspd$: wind speed (m/s)

w_1, w_2, w_3 : coefficients

c : constant

The average of each of these coefficients computed from the field data is shown in the Table 1

Table 1 Tang's model average temperature coefficients for mono-Si Glass/Polymer modules

	w_1	w_2	w_3	c
Average Value	0.942	0.028	-1.509	3.9

The third thermal model just containing the dependence on ambient temperature and irradiance is shown in equation below

$$T_{mod} - T_{amb} = m \times E + b$$

Where

T_{mod}: module Temperature (°C)

T_{amb}: ambient temperature (°C)

E: solar irradiance (W/m^2)

m and b: coefficients

The coefficients m and b range from 0.0054 to 0.0094 and 0.5 to 1.5 at wind speeds of 0.25 to 9.25 m/s, respectively, based on field data.

A brief overview of several thermal models has been presented and the results from the generated thermal model will be compared with the results from these existing thermal models and experimental data for validation

2.3 Standards Regarding Temperature of PV Modules

Even though measurement at Standard Test Condition (STC) has become an industry standard for module name plate data, it is not an accurate representation of real field operating conditions. There are several other temperature measurements which complement the standard test condition (STC) which are conducted in accordance with IEC 61215, IEC 61730-2 and UL 1703 standards. One such measurement used in this work is nominal operating cell temperature (NOCT) as described in IEC 61215 standard [9].

2.3.1 Measurement of NOCT – IEC 61215

For the past few decades, manufacturers used the performance data at Standard Test Condition to rate the modules for market use. Since the modules rarely operate at Standard Test Condition temperature of 25°C, the standard required the manufacturers to provide module temperature at NOCT in addition to STC. The procedure for measurement of NOCT has been provided in the standard IEC 61215 [9]. NOCT can be defined as equilibrium average cell temperature for an open-rack mounted module at Standard Reference Environment (SRE) as stated in IEC standard 61215. The Standard Reference Environment conditions for NOCT is stated in the Table 2

Table 2 Reference conditions for NOCT

Tilt Angle	45° with respect to horizontal
Irradiance	800 W/m^2
Ambient Temperature	20°C
Wind speed	1 m/s
Electrical condition	Open-circuit

2.4 ΔT ($T_{cell} - T_{module}$) Measurement

The IEC-61853 standard [10] requires power measurements including I_{sc}, V_{oc}, V_{max}, P_{max} to be performed at 23 different combinations of temperature and irradiance. Since performing outdoor measurements based on specified set conditions is difficult, performing these measurements in an indoor solar simulator is relatively easier. In the case of indoor solar simulator measurements, the substrate temperature and the cell temperature remains the same since the effect of solar heating is eliminated as the light is flashed only for a few milliseconds. On the other hand, there is an obvious difference between the cell and substrate temperature for measurements performed outdoor. It is important that this temperature difference has to be taken into account to correct for the indoor solar simulator power measurements parameters. Kuitche et al [11] has reported a temperature difference of 1.4 to 2.6 °C between backsheet and cell depending type of sensor used.

2.5 Survey of Different Substrates

The two of the most commonly used substrates for crystalline silicon modules are polymer backsheets and glass. The main objectives of the substrates are to provide electrical insulation, structural stability and moisture impermeability. The thermal properties of a substrate have some effect on the PV module performance. Backsheets with better thermal properties such as good heat dissipation rate or higher thermal conductivity can effectively reduce the operating temperature. Hence a lot of commercially available backsheets all over the world were surveyed [12]. The samples of the backsheets, which seemed to be thermally conductive from their material configuration and properties listed in the specification sheet, were collected and tested for thermal conductivity. Finally, three backsheet materials of varying thermal conductivities were selected for the project. For the

coupons with glass substrate, the same glass material which was used as a superstrate in the fabrication of coupons was used.

3.0 METHODOLOGY

3.1 Procurement of Materials and Design of Single Cell Coupons

3.1.1 Procurement of Materials

3.1.1.1 Backsheets

Since the project aims at evaluating the difference between cell and backsheet temperature, it is important to use backsheets of different thermal conductivities in the study. Hence commercially available backsheets of different material configurations were surveyed and three of them were down-selected based on thermal conductivity, performance and safety certifications.

3.1.1.2 Glass

Glass has been used as both superstrate and substrate in this project. The glass used in this project is inside-textured cerium-free solar glass of 3.2 mm thickness and dimensions 8 × 11 inches.

3.1.1.3 Encapsulant

Ethylene Vinyl Acetate (EVA) has been used as encapsulant material.

3.1.1.4 Tabbing and Bus Bars

The description regarding the size and type of tabbing and bus bars is shown in Table 3

Table 3 Tabbing and bus ribbons specifications

	Size	Solder type (Sn/Pb)	Coating thickness
Tabbing wire	1.50 x 0.15 mm	60/40	10-18 um
Bus wire	5.00 x 0.20 mm	60/40	10-18 um

3.1.1.5 Potting Material for Junction Box

Silicone sealant has been used as adhesive to attach the junction box on to the substrate and it is also used as the potting material to completely fill the junction box cavity and this sealant has a curing time of nearly 24 hours.

3.1.1.6 Solar Cell

Solar cell is a monocrystalline silicon cell of dimensions 15.6 mm x 15.6 mm. The cell is resistant to potential induced degradation.

3.1.1.7 Junction Box

Junction box from Renhe solar has been used for single-cell coupon fabrication in this study. This junction box is of inner-side soldering type and it has a clip-on lid to close the junction box.

3.1.2 Design of Single Cell Coupon

The single cell coupon has been designed in such a way that the cell is at least 1.5 inches away from the junction box for a better thermal distribution throughout the coupon as the heat will be generated from both the cell and junction box. The design of the coupon is clearly illustrated in the Figure 1

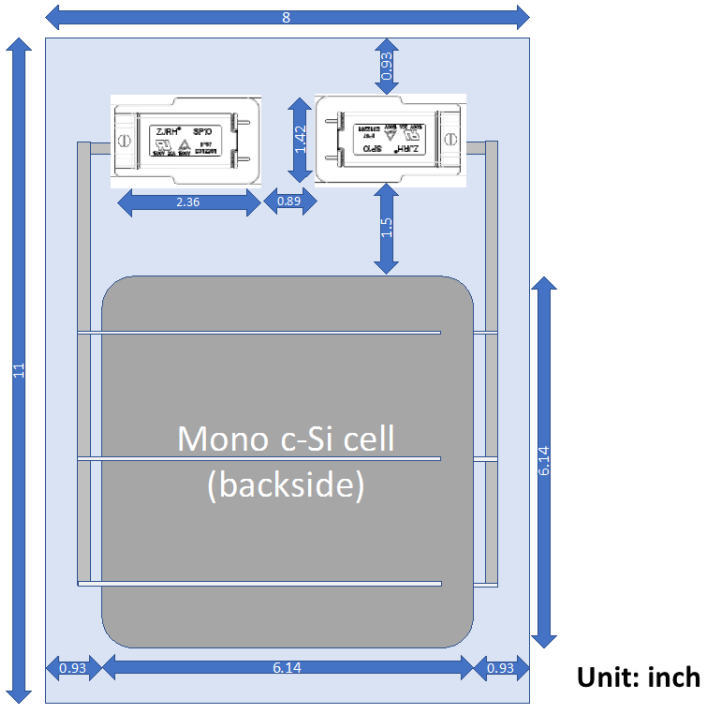

Figure 1 Design of single cell coupon

3.2 Fabrication of Single Cell Coupon

3.2.1 Tabbing and Interconnect Soldering

A spool of tabbing ribbon was initially setup into a spool tensioner in order to facilitate easy handling. The tabbing ribbons from the tensioner were pre-cut to required size. The tabbing ribbons were dipped in Kester 952 S Flux solution and allowed to dry at the room temperature and then placed into the semi-automated tabbing machine as shown in Figure 2.

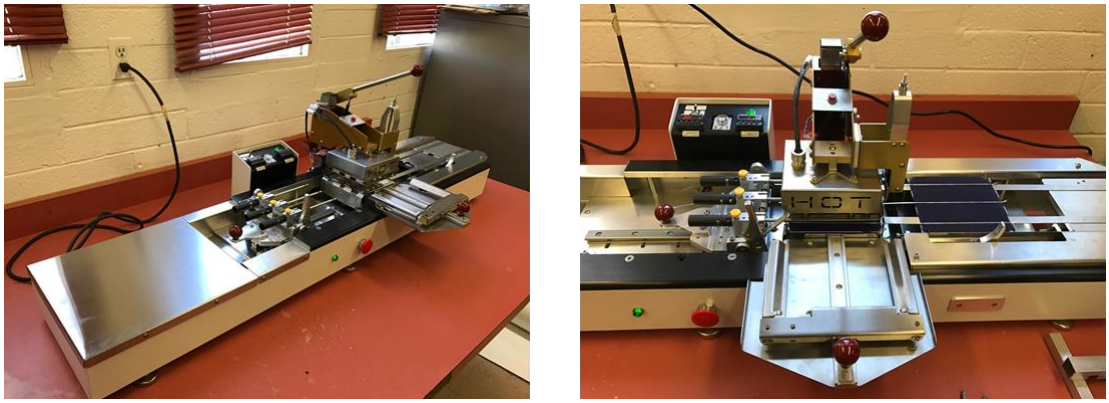

Figure 2 Semi-automated tabbing machine

The front side of the cell was soldered using the semi-automated tabbing machine. The soldering with semi-automated tabbing machine was performed only after the heater reaches preset temperature of 235 °C. The pressing time for front-side tabbing is approximately 2 s**.** The back side of the cell was soldered manually due to alignment issues in the tabbing machine. The interconnect bus ribbons leading to the junction box were also soldered manually. The soldered cells are shown in Figures 3,4,5,6.

Figure 3 Front side of soldered cell

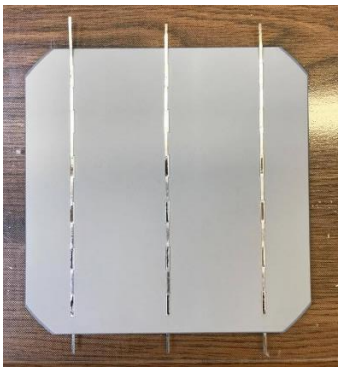

Figure 4 Rear side of soldered cell

Figure 5 Completed soldered cell

Figure 6 Soldered cell for glass-glass Coupon

3.2.2 Preparation of Glass, Backsheet and Encapsulant Materials

Both the sides of the glass were thoroughly cleaned using isopropyl alcohol. The backsheet and encapsulant were cut at the same dimensions as that of the glass. For each coupon fabrication, one backsheet and two EVA sheets were cut. Two slits for bus ribbons coming out from the cell were made in the EVA sheets and the backsheet

3.2.3 Module Lamination

It must be noted that since the project involves monitoring on-field cell temperature as well, a very thin thermocouple wire was placed on the backside of the solar cell right before the process of lamination. The layers were stacked up as follows to laminate the coupons. Textured side of glass facing up, encapsulant with smooth side down, cell (with interconnect ribbons) with backside facing up, soldered end of thermocouple wire, encapsulant with smooth side down, outside of the backsheet facing up. The stacking up process is same for coupons with glass substrates except for glass in the place of backsheet. This stacked up arrangement was placed between two PTFE release sheets and then placed in the laminator as shown in Figure 7. The lamination was performed at a temperature of 150 °C and vacuum pressure for nearly 20 minutes. Two coupons were fabricated in a single lamination process. After the lamination is done, the coupons were allowed to cool down for 10 minutes before removing from the laminator as shown in Figure 8. The coupons before and after lamination are shown in Figures 9, 10, 11, 12.

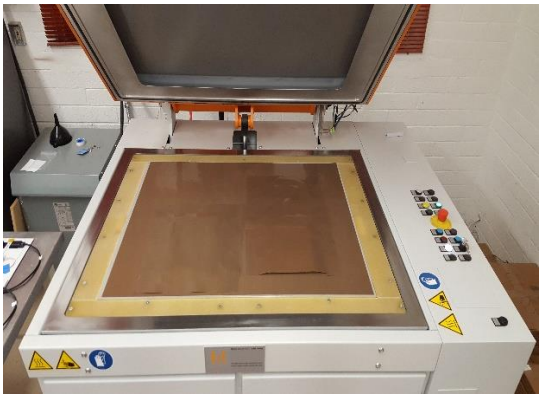

Figure 7 Laminator with cover open

Figure 8 Laminator with control system

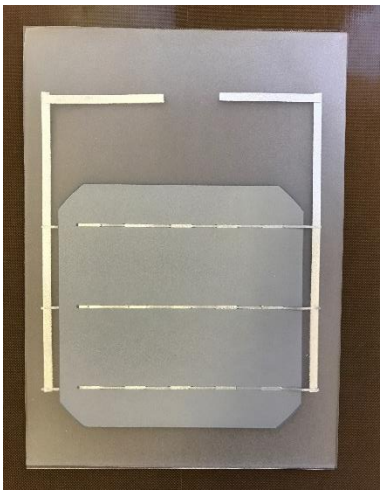

Figure 9 Stacked up materials of glass-polymer coupon before lamination

Figure 10 Glass-Polymer coupon after lamination

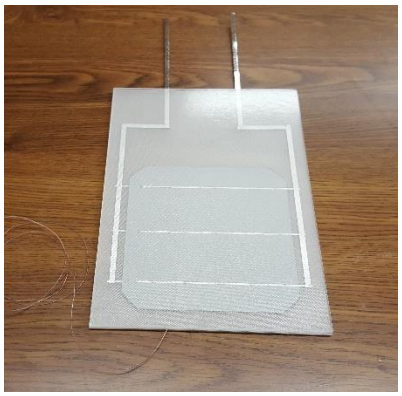

Figure 11 Stacked up glass-glass coupon materials before lamination

Figure 12 Glass-Glass coupon after lamination

3.2.4 Junction Box Attachment

Junction box was attached on to the backside of the coupon using PV-804 Dow Corning sealant. The bus ribbons coming from the cell were soldered inside the junction box and the junction box cavity was completely filled with the potting material (same as that of the sealant) and allowed to cure for at least 48 hours at room temperature shown in Figures 13 and 14. After curing, the lid is snapped on to close the junction box. The front and back views of a coupon is shown in figures 15 and 16. During initial I-V measurements, the coupons were found to have very low fill factor caused by high series resistance. But when the I-V measurement was performed without the connectors, the fill factor increased by 5 %. This might be due to high resistance metal contact used in the connectors. Hence the connectors were chopped off and the ends were protected with wire nuts when installed in the field. The fully fabricated coupon with connector is shown in Figure 17.

Figure 13 Junction box cavity filled with sealant (glass-glass coupon)

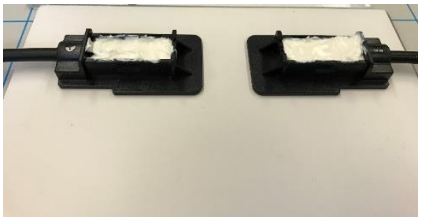

Figure 14 Junction box cavity filled with sealant (glass-polymer coupon)

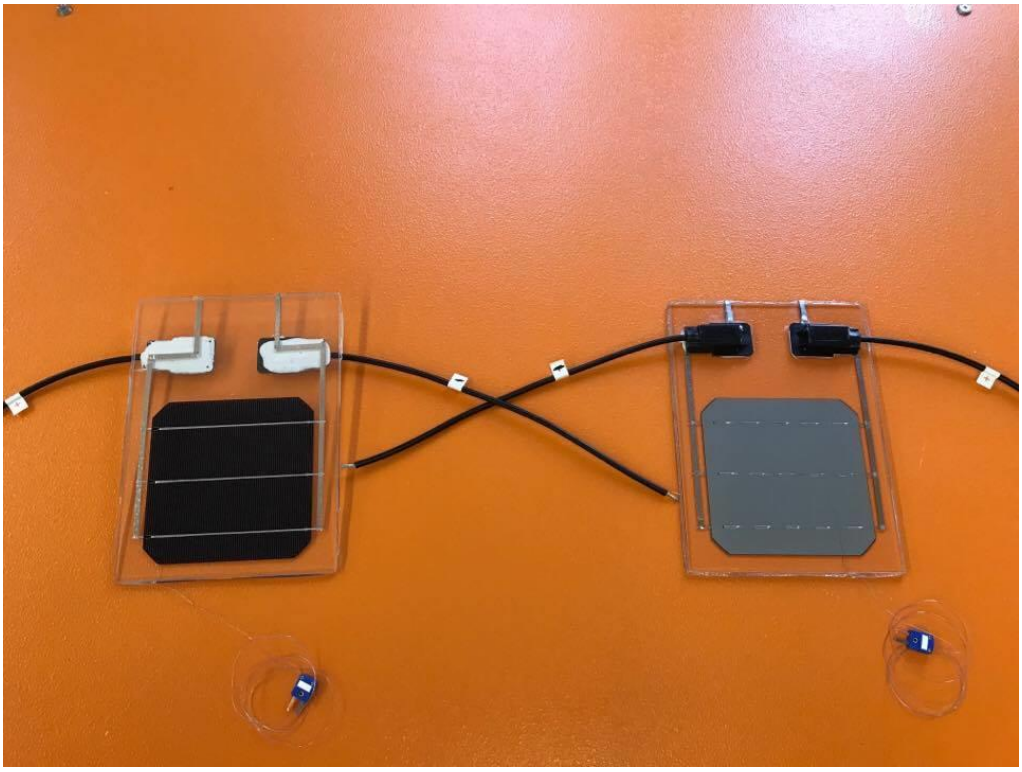

Figure 15 Front and back view of glass - glass coupon with thermocouple attached

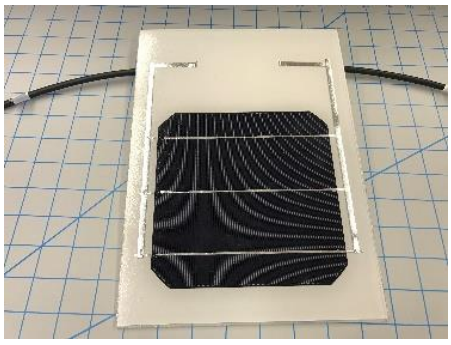

Figure 16 Front view of glass - polymer coupon

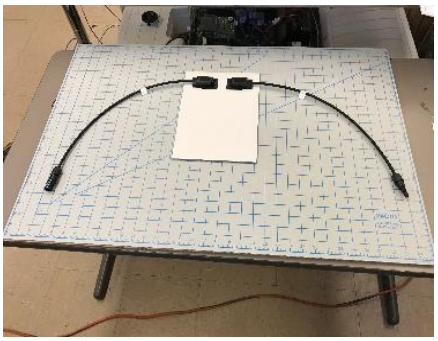

Figure 17 Rear view of glass - polymer coupon with Junction box and connectors

3.3 Design, Fabrication, Installation and Commissioning of the Test Setup

3.3.1 Design and Fabrication of NOCT Rack

The rack for mounting the test coupons was built using 80-20 T-slotted framing extrusions. The design of the rack is in compliance with IEC 61215 standard for NOCT measurement. The coupon is mounted at a height of nearly 4 feet from the ground and the tilt angle to the horizontal is 45°. Each row in the rack can hold up to 12 coupons and the rack comprises of 3 rows.

3.3.2 Data Acquisition System

The data acquisition system consists of Campbell scientific CR1000 data logger and AM 16/32 multiplexers. The CR1000 data logger as shown in the figure 18 consists of a measurement, control module and wiring panel and it requires use of external keyboard and display unit. RS232 port provided in CR1000 was used to connect the DAS to external computer for data transfer or programming modifications.

Figure 18 CR1000 data acquisition system

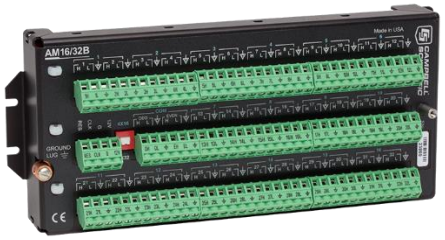

Figure 19 16x32 multiplexer

AM 16/32 channel relay multiplexer was used in order to increase the number of sensors the datalogger can measure. AM 16/32 is shown in the figure 19. The multiplexer was controlled by CR1000 data logger through a control port. Each coupon has two thermocouples (one for backsheet temperature and another one for cell temperature measurement) and one set of high and low voltage measurements. Hence three sets of high and low ports are required for each coupon in the wiring panel. Since there are 8 coupons, 24 ports are required in total. The multiplexer has 32 ports and it is sufficient enough to record the data from all the input lines. Each port in the wiring panel was programmed to record specific set of data such as temperature and voltage using Campbell scientific DAS software Logger net and the on-field DAS wiring was done according to wiring diagram generated from Logger net program. The DAS is powered by AC power source in the test field. The Complete DAS setup with wiring is shown in the figure 20.

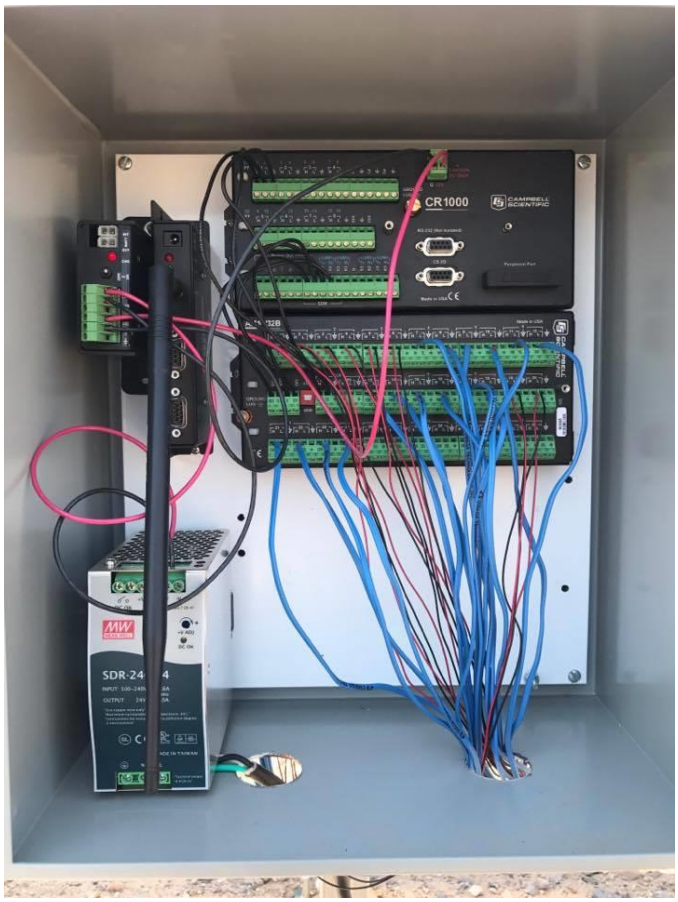

Figure 20 DAS setup in the field

3.3.3 Voltage and Temperature Measurement

T-type thermocouple with sub-miniature molded connector and Kapton insulated wire of size AWG 30 was attached approximately at the center of substrate surface using thermally insulative Kapton tape for substrate temperature measurement. The same T-type thermocouple with Kapton insulated wire of size AWG 36 was used for cell temperature measurement and it was integrated inside the coupon right before the process of lamination. The male thermocouple connector was connected to the free end of thermocouple wire coming out from the coupon after the lamination process. In order to connect the thermocouples to the DAS, the male connectors of thermocouples from the coupon were

connected to female connectors of the thermocouple wires going into the DAS. For voltage measurements, two insulated wires each for positive and negative lines were attached to one wire nut each and the positive and negative terminal lines from the coupon were the attached to corresponding line wires through wire nut which eventually runs into the DAS.

3.3.4 Ambient Conditions Measurement

Since this project aims at predicting the role of ambient conditions in the temperature and voltage output from the coupons, it is very important to accurately measure the ambient conditions such as irradiance, ambient temperature, windspeed and wind direction at the place where the test rack is installed. Since the coupons are tilted at 45°, it is important to measure plane of array irradiance. Hence a pyranometer was installed at 45° tilt angle in the weather station near the test rack. All other data such as ambient temperature, windspeed and wind direction were obtained from the respective sensors installed in the weather station. The weather station which is to the north of the rack is shown in the Figures 21 and 22.

Figure 21 Front view of weather station in the field

Figure 22 Rear view of weather station in the field

3.3.5 Installation and Commissioning of Test Rack

The test rack has been installed to the south of weather station in the ASU-PRL's test field. It was nailed down to the ground using L-clamps. Two L-clamps were deployed for each of the T-slotted framing extrusions which form the base of the rack. The coupons were installed on to the rack side by side using adjustable end clamps. The DAS setup is mounted at the back of NOCT rack and is tightly fixed on to the rack using appropriate fasteners. After completely checking the working of all sensors and data acquisition system, coupons, structural and electrical safety of the test setup, the test rack was commissioned to collect data required for further analysis and modeling. The test rack is shown in Figures 23, 24 and 25.

Figure 23 Installed Coupons in the test rack

Figure 24 Front view of test rack

Figure 25 Rear view of test rack

3.4 Module Characterization

3.4.1 Light Soaking

The fabricated coupons were exposed to sunlight for two straight sunny days getting at least 10 kWh/m^2 as required by the IEC 61215 standard for the removal of light induced degradation. The insolation for day 1 was 5.5 kWh/m^2 and insolation for day 2 was 5.2 kWh/m^2.

3.4.2 I-V Curve Measurements

An indoor class A solar simulator was used for taking I-V measurements on the already light soaked coupons. Dark I-V curves and light I-V curves were obtained at two irradiance levels (~230 and 1000 W/m^2) for all the coupons. As an example, Table 4 shows the I-V data for three coupons at STC (standard test conditions): one coupon of each backsheet type.

Table 4 I-V measurements of coupons

Backsheet Type	Isc (A)	Voc (V)	Imp (A)	Vmp (V)	Pmax (W)	Fill Factor (%)	Efficiency (%)
Type 1	8.902	0.626	8.094	0.4285	3.469	62.2	14.51
Type 2	8.975	0.625	8.067	0.4269	3.444	61.4	14.41
Type 3	8.744	0.623	7.995	0.4218	3.372	61.9	14.11

3.4.3 Electroluminescence Imaging

Electroluminescence images were taken for all coupons. Figure 26 shows the EL images from three sample coupons

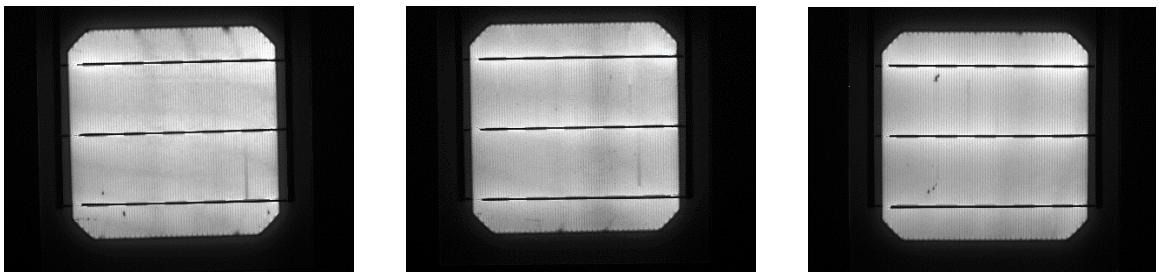

Figure 26 EL images of sample coupons

3.4.4 Infrared Imaging

In a dark room environment, the coupon was supplied 8 A using a power supply. After two minutes, infrared images of front and back of each coupon as shown in Figure 27 was taken using an infrared camera.

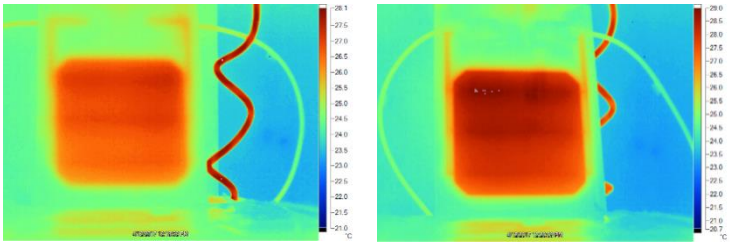

Figure 27 IR Images of front and back side of a sample coupon

3.4.5 Spectral Reflectance

For measuring the spectral reflectance at the same position for all coupons, a masking sheet with the same size as that of coupon with open space right near the center of the cell was used. The reflectance was measured on the surface of backsheet using a handheld spectrophotometer. The spectrum reflectance graph one for each coupon of different backsheet is shown in the Figure 28. In the graph, the wavelength is indicated in nanometers.

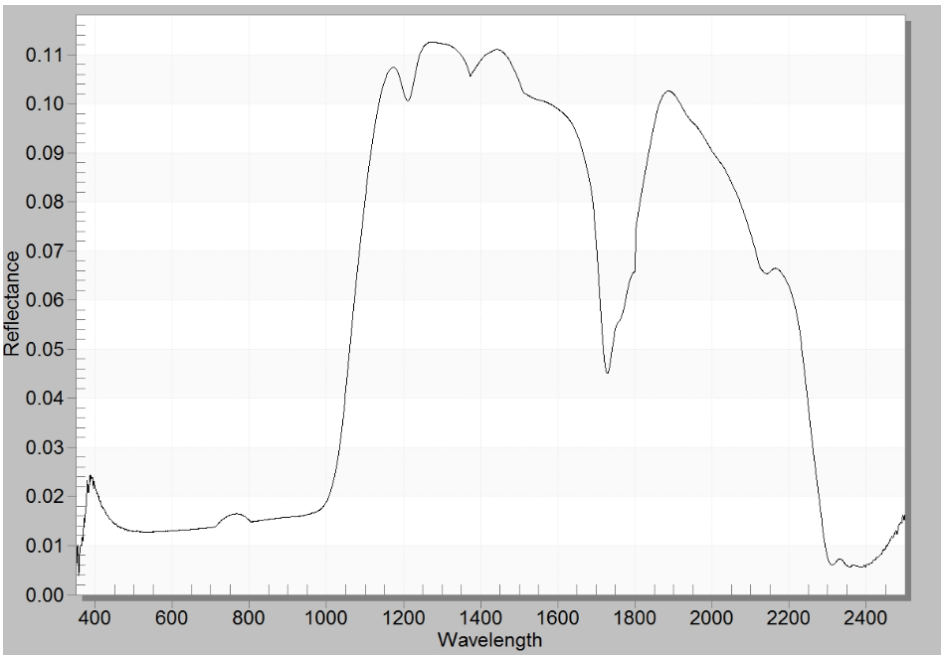

Figure 28 Spectral reflectance of front side of the coupon

3.5 Backsheet Characterization

3.5.1 Thermal Conductivity Measurement

The samples were tested for thermal conductivity using Hot Disk TPS 2500 S. Each sample was cut to size 2 cm x 2 cm. The values of heat capacity were included in to the measurement system. Prior to the conductivity measurements, the heat capacities of the samples were measured using TPS specific heat method at the Thermtest testing lab. A few minutes after heat flows from the sensor/heating element on to the sample, thermal conductivity along with other thermal properties was measured. The thermal conductivities for different backsheet samples determined from the equipment are shown in Table 5

Table 5 Thermal conductivity measurements

Backsheet Type	Bulk Thermal Conductivity (W/m·K)	Axial Thermal Conductivity (W/m·K)	Radial Thermal Conductivity (W/m·K)
Type 1	0.274	0.153	0.486
Type 2	0.305	0.259	0.371
Type 3	2.274	0.382	13.53

4. RESULTS AND DISCUSSION

4.1 Thermal Model for Module and Cell Temperature

4.1.1 Overview

Three mathematical models for predicting module and cell temperature were developed in this study. All the models are linear regression models developed using JMP. The first model takes into account seven input parameters: irradiance, wind speed, ambient temperature, wind direction, relative humidity, axial and radial thermal conductivities of the backsheet. Another model was developed based on input parameters: irradiance, ambient temperature, wind speed, wind direction, relative humidity and bulk thermal conductivity (directionless thermal conductivity). The third model was developed based on just the ambient conditions: irradiance, ambient temperature, wind speed, wind direction and relative humidity

4.1.2 Thermal Model #1

This model has a format as shown in the equation below. The seven input parameters for this model are irradiance, ambient temperature, wind speed, wind direction, relative humidity, axial and radial thermal conductivity.

The equation is as follows

$$T_{mod}\ or\ T_{cell} = w_1 \times T_{amb} + w_2 \times E + w_3 \times Windspd + w_4 \times WD + w_5 \times RH + w_6 \times Ka + w_7 \times kr + c$$

Where,

T_{cell}: cell temperature (°C)

T_{mod}: module or substrate temperature (°C)

T_{amb}: ambient temperature (°C)

E: irradiance (W/m^2)

$Windspd$: wind speed (m/s)

WD : wind direction (degrees)

RH : relative humidity (%)

Ka : axial thermal conductivity (W/m/K)

Kr : radial thermal conductivity (W/m/K)

$w_1, w_2, w_3, w_4, w_5, w_6, w_7$: coefficients

c : constant

The coefficients obtained for mono crystalline silicon coupons based on field data are shown in the Table 6

Table 6 Model Coefficients for Model #1

	T_{amb}	E	Windspd	WD	RH	Ka	Kr	c
T_{mod}	1.045	0.027	-1.634	0.0001	0.044	-1.245	0	-0.707
T_{cell}	1.041	0.031	-1.413	0.0022	0.048	-1.795	0	-1.390

This table is based on 7 AM to 6 PM data from May 1-31, 2017 (excluding May 8, 2017), June 9 - July 12, 2017 (excluding June 12, July 5, July 11)

It can be interpreted from the Table 6 that the module and cell temperature are mainly driven by ambient temperature while irradiance and windspeed also have some significant contribution to the module and cell temperature. As expected, radial thermal conductivity has no role to play while wind direction, relative humidity and axial thermal conductivity have a small contribution to module temperature and cell temperature. To evaluate the performance of this model, comparisons was made between the measured and predicted values using data from all coupons with backsheet substrate. The results of the comparisons are shown in the Figures 29 and 30.

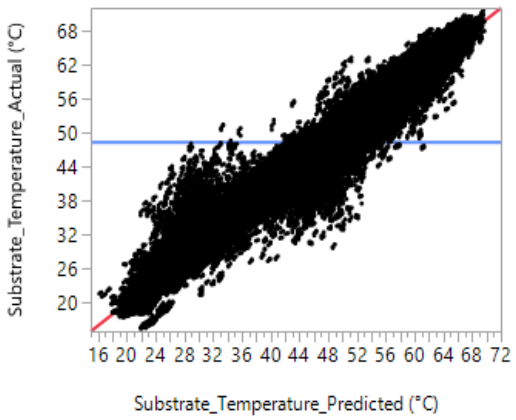

R^2 Value
0.96

Figure 29 Evaluation of model #1 - backsheet temperature

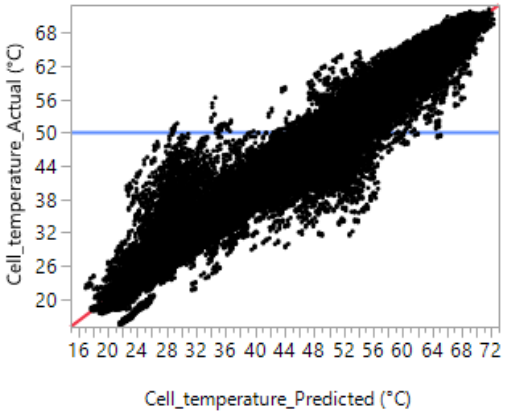

R^2 Value
0.97

Figure 30 Evaluation of model #1 - cell temperature in (°C)

4.1.3 Thermal Model #2

This thermal model has the format as shown in the equation below. This model is almost same as the previous model except that thermal conductivity considered in this model is directionless and it is called bulk thermal conductivity. The equation is as follows

$$T_{mod}\ or\ T_{cell} = w_1 \times T_{amb} + w_2 \times E + w_3 \times Windspd + w_4 \times WD + w_5 \times RH + w_6 \times K + c$$

Where,

T_{cell}: cell temperature (°C)

T_{mod}: module or substrate temperature (°C)

T_{amb}: ambient temperature (°C)

E: irradiance (W/m^2)

$Windspd$: wind speed (m/s)

WD : wind direction (degrees)

RH : relative humidity (%)

K : bulk thermal conductivity (W/m/K)

$w_1, w_2, w_3, w_4, w_5, w_6$: coefficients

c : constant

The coefficients obtained for mono crystalline silicon coupons based on field data are shown in the Table 7

Table 7 Model Coefficients for model #2

	T_{amb}	E	Windspd	WD	RH	K	c
T_{mod}	1.045	0.027	-1.634	0.0002	0.044	-0.143	-0.222
T_{cell}	1.041	0.031	-1.413	0.002	0.048	-0.205	-1.608

This table is based on 7 AM to 6 PM data from May 1-31, 2017 (excluding May 8, 2017), June 9 - July 12, 2017 (excluding June 12, July 5, July 11)

Just like the previous model, it can be interpreted from the Table 7 that both the module and cell temperatures are mainly driven by ambient temperature, irradiance and wind speed and slightly or negligibly affected by wind direction and relative humidity. The contribution of bulk thermal conductivity is almost same as that of axial thermal conductivity. To evaluate the performance of this model, comparison was made between the measured and predicted values using data from all coupons with backsheet substrate. The results of the comparisons are shown in the Figures 31 and 32

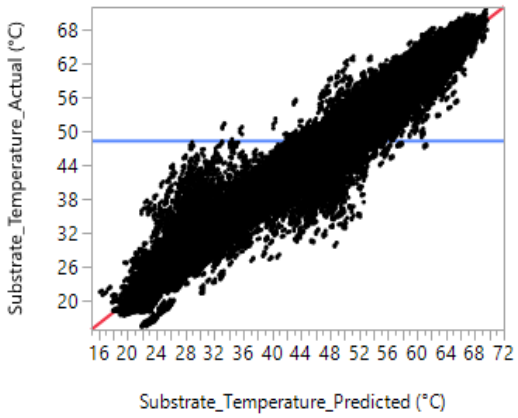

R^2 Value
0.97

Figure 31 Evaluation of model #2 - backsheet temperature in (°C)

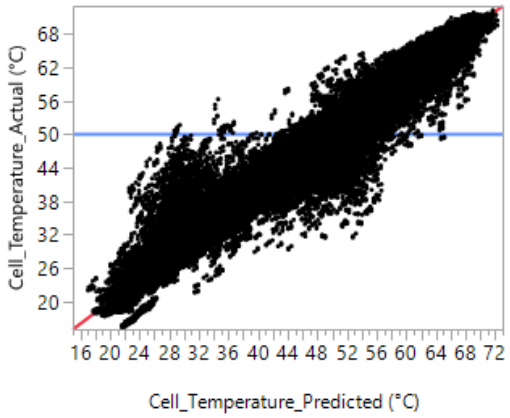

R^2 Value
0.97

Figure 32 Evaluation of model #2 - cell temperature in (°C)

4.1.4 Thermal Model #3

This thermal model has the format as shown in the equation. This model is just based on ambient conditions.

The equation is as follows

$$T_{mod}\ or\ T_{cell} = w_1 \times T_{amb} + w_2 \times E + w_3 \times Windspd + w_4 \times WD + w_5 \times RH + c$$

Where,

T_{cell}: cell temperature (°C)

T_{mod}: module or substrate temperature (°C)

T_{amb}: ambient temperature (°C)

E: irradiance (W/m^2)

$Windspd$: wind speed (m/s)

WD : wind direction (degrees)

RH : relative humidity (%)

w_1, w_2, w_3, w_4, w_5 : coefficients

c : constant

The coefficients obtained for each coupon with different substrate based on field data are shown in the Tables 8 and 9. The average coefficients for all the coupons are also listed in Tables 8 and 9. To evaluate the performance of this model, comparison was made between

the measured and predicted values using data from all coupons with backsheet and glass substrate. The results of the comparisons are shown in the Figures 33, 34, 35, 36, 37, 38, 39 and 40.

Table 8 Model coefficients for module or substrate temperature

Substrate	Module	T_{amb}	E	Windspd	WD	RH	c
Backsheet Type 1	1	1.047	0.027	-1.664	0.0002	0.042	-0.227
	2	1.043	0.027	-1.573	0.0001	0.045	-0.468
	Average	1.045	0.027	-1.619	0.0001	0.043	-0.347
Backsheet Type 2	1	1.033	0.025	-1.645	-0.003	0.038	0.745
	2	1.037	0.027	-1.658	-0.001	0.043	0.115
	Average	1.035	0.026	-1.651	-0.002	0.041	0.430
Backsheet Type 3	1	1.041	0.027	-1.673	-0.0002	0.047	-0.559
	2	1.049	0.027	-1.624	0.0005	0.039	-0.359
	Average	1.045	0.027	-1.648	0.0001	0.043	-0.459
Overall average		1.042	0.027	-1.639	0.0006	0.042	-0.125
Glass	1	0.976	0.027	-1.414	0.0004	0.020	2.666
	2	1.036	0.029	-1.316	0.004	0.008	-0.420
	Average	1.006	0.028	-1.365	0.0022	0.014	1.123

This table is based on 7 AM to 6 PM data from May 1-31, 2017 (excluding May 8, 2017), June 9 - July 12, 2017 (excluding June 12, July 5, July 11).

Table 9 Model coefficients for cell temperature

Substrate	Module	T_{amb}	E	Windspd	WD	RH	c
Backsheet Type 1	1	1.043	0.032	-1.456	0.003	0.046	-1.638
	2	1.035	0.031	-1.355	0.001	0.048	-1.665
	Average	1.039	0.031	-1.405	0.002	0.047	-1.652
Backsheet Type 2	1	1.033	0.029	-1.469	-0.001	0.045	-0.745
	2	1.039	0.031	-1.449	-0.001	0.048	-1.600
	Average	1.036	0.030	-1.459	-0.001	0.046	-1.173
Backsheet Type 3	1	1.038	0.032	-1.439	-0.001	0.055	-2.206
	2	1.049	0.031	-1.401	0.003	0.044	-1.972
	Average	1.043	0.031	-1.420	0.001	0.049	-2.089
Overall average		1.039	0.031	-1.428	0.0006	0.047	-1.638
Glass	1	0.990	0.032	-1.199	0.002	0.023	0.594
	2	1.032	0.033	-1.090	0.006	0.009	-1.899
	Average	1.011	0.032	-1.144	0.004	0.016	-0.652

This table is based on 7 AM to 6 PM data from May 1-31, 2017 (excluding May 8, 2017), June 9 - July 12, 2017 (excluding June 12, July 5, July 11).

To evaluate the performance of this model, comparisons were made between the measured and predicted values for the coupons with different substrates separately.

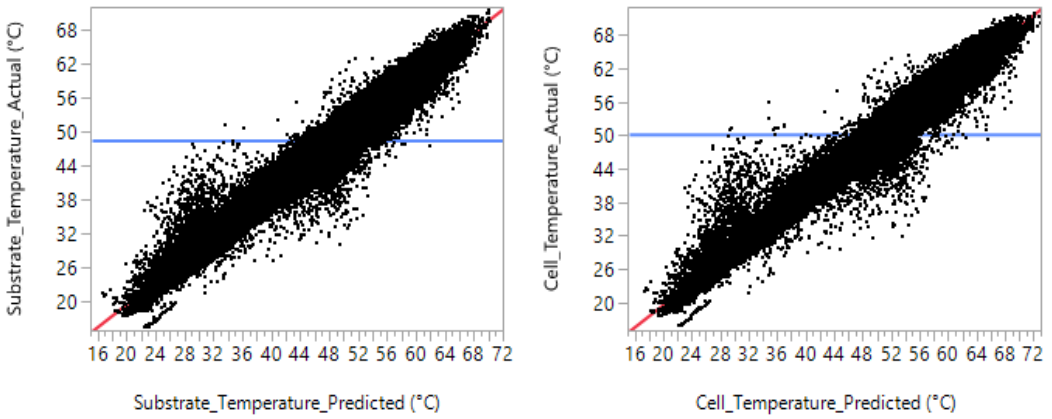

R^2 Value = 0.97

R^2 Value = 0.97

Figure 33 Evaluation of model #3 for coupon 1 of backsheet type 1 - backsheet (left) and cell (right) temperatures in °C

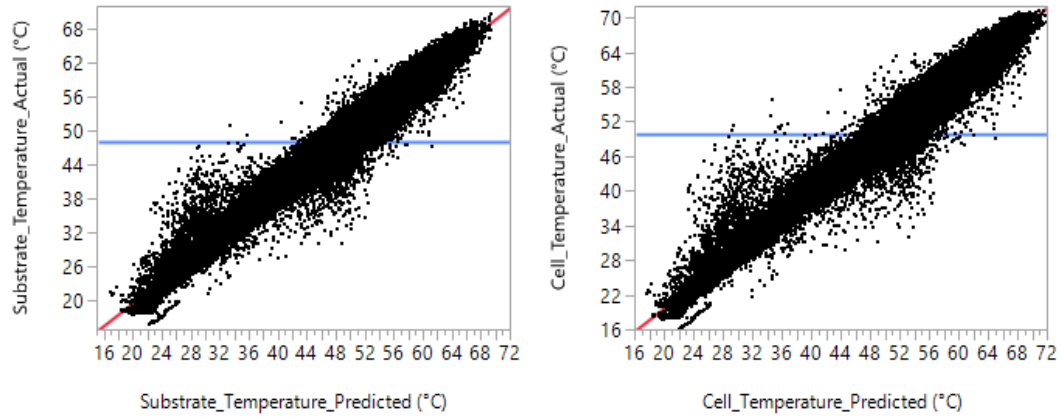

R^2 Value = 0.96

R^2 Value = 0.97

Figure 34 Evaluation of model #3 for coupon 2 of backsheet type 1 – backsheet (left) and cell (right) temperatures in °C

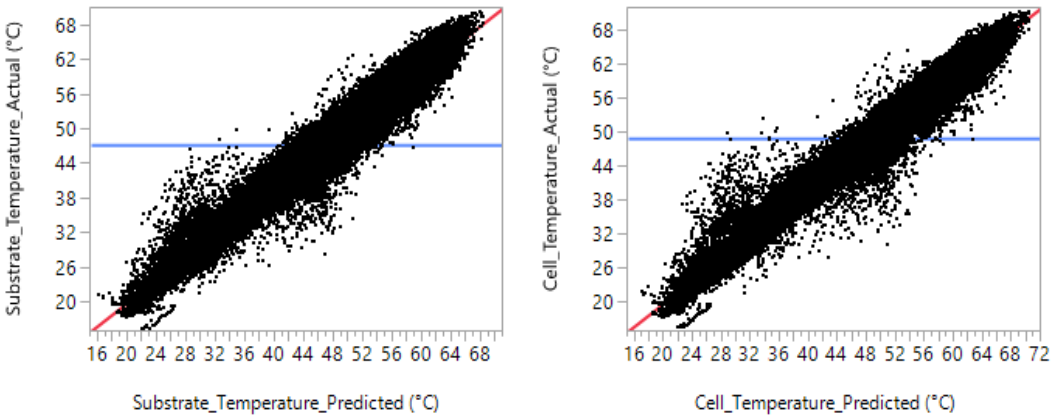

R^2 Value = 0.96

R^2 Value = 0.96

Figure 35 Evaluation of model #3 for coupon 1 of backsheet type 2 - backsheet (left) and cell (right) temperatures in °C

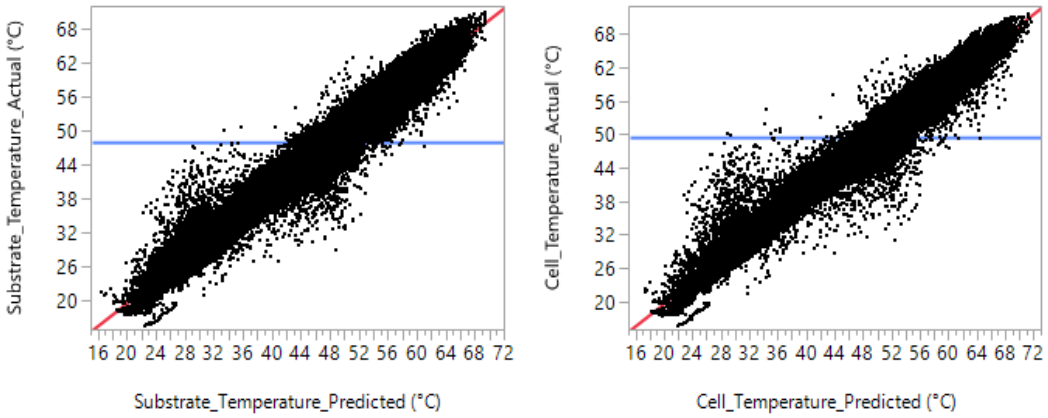

R^2 Value = 0.96

R^2 Value = 0.97

Figure 36 Evaluation of model #3 for coupon 2 of backsheet type 2 – backsheet (left) and cell (right) temperatures in °C

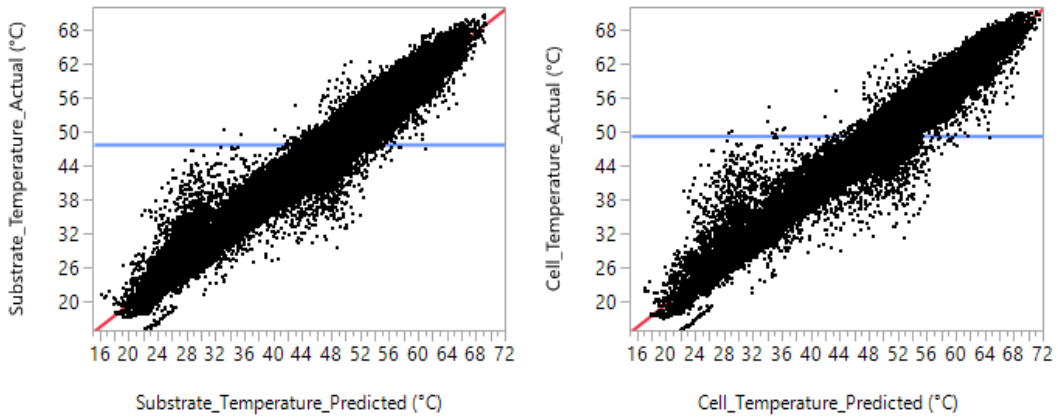

R^2 Value = 0.96

R^2 Value = 0.97

Figure 37 Evaluation of model #3 for coupon 1 of backsheet type 3 - backsheet (left) and cell (right) temperatures in °C

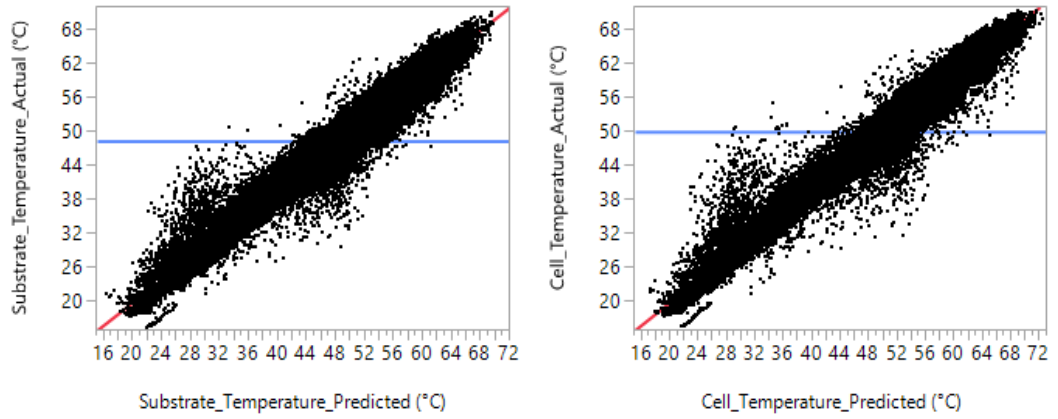

R^2 Value = 0.96

R^2 Value = 0.97

Figure 38 Evaluation of model #3 for coupon 2 of backsheet type 3 – backsheet (left) and cell (right) temperatures in °C

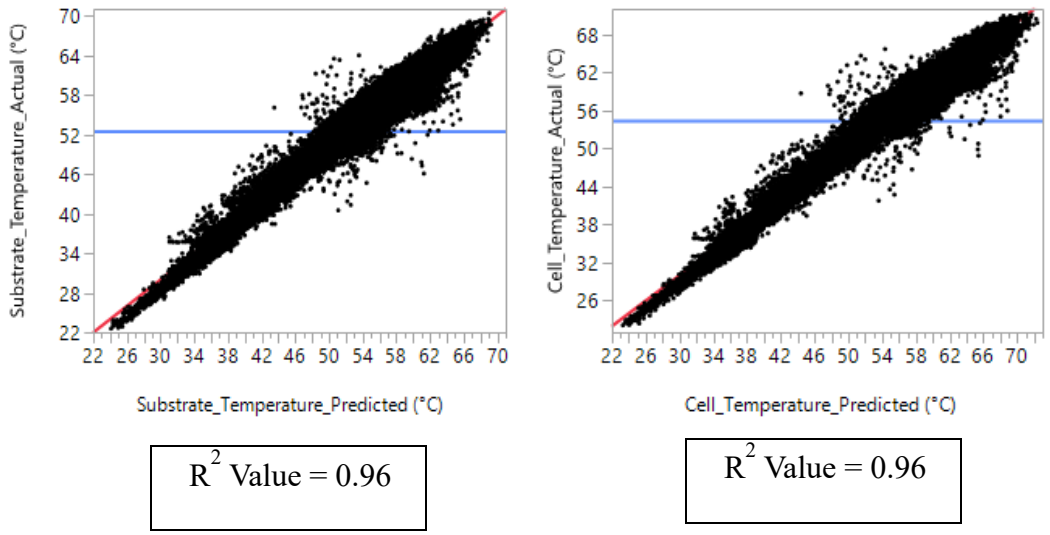

Figure 39 Evaluation of model #3 for Glass-Glass coupon 1 - backsheet (left) and cell (right) temperatures in °C

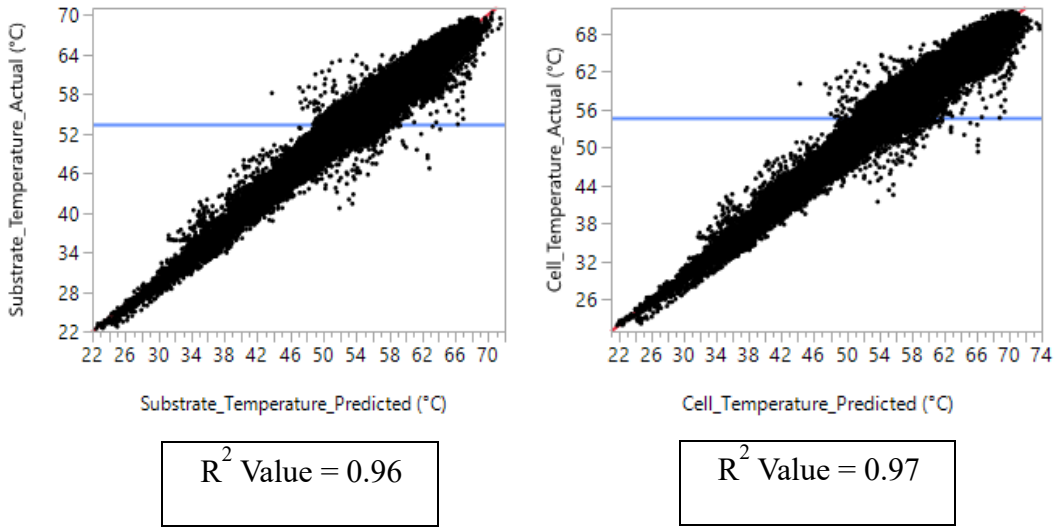

Figure 40 Evaluation of model #3 for Glass-Glass coupon 2 – backsheet (left) and cell (right) temperatures in °C

4.2 Evaluation of Thermal Models

All the models presented are linear regression models developed based on field data from May 1-31, June 9-30 and July 1-12. They satisfy all the linear regression assumptions except for auto-correlation. Hence these models might perform better only during summer months. Analysis of all three thermal models is presented in this section.

4.2.1 Thermal Model #1 and #2

These two models have managed to capture the effect of thermal conductivity of the backsheet in to account. Even though the effect of thermal conductivity is considerably small compared to other major factors like ambient temperature, irradiance and windspeed, increase in axial thermal conductivity by 1 W/m/K could reduce the module temperature by 1.2°C and cell temperature by 1.8°C. Since the radial component of thermal conductivity has zero significance on both the module and cell temperatures, knowing axial thermal conductivity of the backsheet helps in better prediction of operating temperature rather than the second thermal model which uses bulk thermal conductivity. The thermal model equations for predicting the module and cell temperatures if axial thermal conductivity is known are given as follows

$$T_{mod} = 1.045 \times T_{amb} + 0.027 \times E - 1.634 \times Windspd + 0.0001 \times WD + 0.044 \times RH - 1.245 \times Ka - 0.707$$

$$T_{cell} = 1.041 \times T_{amb} + 0.031 \times E - 1.413 \times Windspd + 0.0022 \times WD + 0.048 \times RH - 1.795 \times Ka - 1.390$$

Where,

T_{cell}: cell temperature (°C)

T_{mod}: module or substrate temperature (°C)

T_{amb}: ambient temperature (°C)

E: irradiance (W/m^2)

$Windspd$: wind speed (m/s)

WD : wind direction (degrees)

RH : relative humidity (%)

Ka : axial thermal conductivity (W/m/K)

4.2.2 Thermal Model #3

In the case of coupons with backsheet as substrate, the module temperature is primarily dictated by ambient temperature. The base temperature of the module is set by ambient temperature and then irradiance is responsible for the module temperature rise at about 0.027°C per W/m^2 and cell temperature rise at about 0.031°C per W/m^2. On the other hand, the module temperature and cell temperature drops by 1.6°C and 1.4°C per m/s wind speed increase. The model with the overall average coefficient set as indicated in the equation below could be used for reliable prediction of module temperature of glass-polymer coupons.

$$T_{mod} = 1.042 \times T_{amb} + 0.027 \times E - 1.639 \times Windspd + 0.0006 \times WD + 0.042 \times RH - 0.125$$

$$T_{cell} = 1.039 \times T_{amb} + 0.031 \times E - 1.428 \times Windspd + 0.0006 \times WD + 0.047 \times RH - 1.638$$

Where,

T_{cell}: cell temperature (°C)

T_{mod}: module or substrate temperature (°C)

T_{amb}: ambient temperature (°C)

E: irradiance (W/m^2)

$Windspd$: wind speed (m/s)

WD : wind direction (degrees)

RH : relative humidity (%)

In the case of coupons with glass as substrate, the module and cell temperatures are predominantly influenced by irradiance as the module and cell temperatures increase 0.028 °C and 0.032 °C per W/m^2. Wind speed plays a lesser significant role in glass-glass coupons compared to glass-polymer coupons. The module temperature and cell temperature drop only by 1.4 °C and 1.1 °C respectively per m/s wind speed increase. The model with the overall average coefficient set as indicated in the equation could be used for reliable prediction of module temperature of glass-glass coupons.

$$T_{mod} = 1.006 \times T_{amb} + 0.028 \times E - 1.365 \times Windspd + 0.002 \times WD + 0.014 \times RH + 1.123$$

$$T_{cell} = 1.011 \times T_{amb} + 0.032 \times E - 1.144 \times Windspd + 0.004 \times WD + 0.016 \times RH - 0.652$$

Where,

T_{cell}: cell temperature (°C)

T_{mod}: module or substrate temperature (°C)

T_{amb}: ambient temperature (°C)

E: irradiance (W/m^2)

$Windspd$: wind speed (m/s)

WD : wind direction (degrees)

RH : relative humidity (%)

4.4 Nominal Operating Cell Temperature Determination and Comparison

Measuring nominal operating temperature (NOCT) requires certain installation conditions like open-rack, tilt angle of 45° and distance of 0.5 m from the ground. Since the test rack meets all the above said conditions, the temperature measurements from the coupons installed in the test rack can be directly used for NOCT determination.

The procedure as listed in IEC 61215 was followed for calculating NOCT for each coupon installed in the test rack. In this study, NOCT has been calculated using both the substrate temperature and cell temperature. The data from June 13, June 14 and June 15, 2017 measurements were considered for NOCT calculation. The 3-day averaged substrate NOCT and cell NOCT obtained for each coupon and R^2 values are shown in the Tables 10 and 11

Figures 41 and 42 show the averaged substrate NOCT and cell NOCT values for coupon of each substrate type. It can be noted from the Figures that coupons with the backsheets which have higher thermally conductivity values are cooler than the backsheets

with lower thermal conductivity in the case of glass-polymer coupons while the glass-glass coupons continue to operate at higher temperature than glass-polymer coupons due to its lower heat dissipation capacity. Interestingly, the thermal conductivity of backsheet 3 is more than that of backsheet 2 but still the coupon with backsheet 3 operates at a higher temperature than coupon with backsheet 2. It can be explained by the fact that backsheet 3 contains a thin layer of aluminum which radiates the absorbed heat onto the cell even though it has better thermal conductivity. This in turn slightly increases both the operating cell and backsheet temperature.

Table 10 NOCT of all coupons - Substrate temperature

Substrate	Module	Substrate NOCT (°C)	R^2 Value
Backsheet Type 1	1	44.8	0.84
	2	44.3	0.85
	Average	44.5	
Backsheet Type 2	1	42.2	0.73
	2	43.9	0.81
	Average	43.0	
Backsheet Type 3	1	43.9	0.84
	2	44.2	0.85
	Average	44.0	
Glass	1	44.5	0.82
	2	46.0	0.90
	Average	45.2	

Table 11 NOCT of all coupons - Cell Temperature

Substrate	Module	Cell NOCT (°C)	R^2 Value
Backsheet Type 1	1	46.7	0.89
	2	47.2	0.90
	Average	46.9	
Backsheet Type 2	1	45.1	0.85
	2	46.5	0.90
	Average	45.8	
Backsheet Type 3	1	46.5	0.91
	2	46.1	0.90
	Average	46.3	
Glass	1	47.5	0.89
	2	48.4	0.92
	Average	47.9	

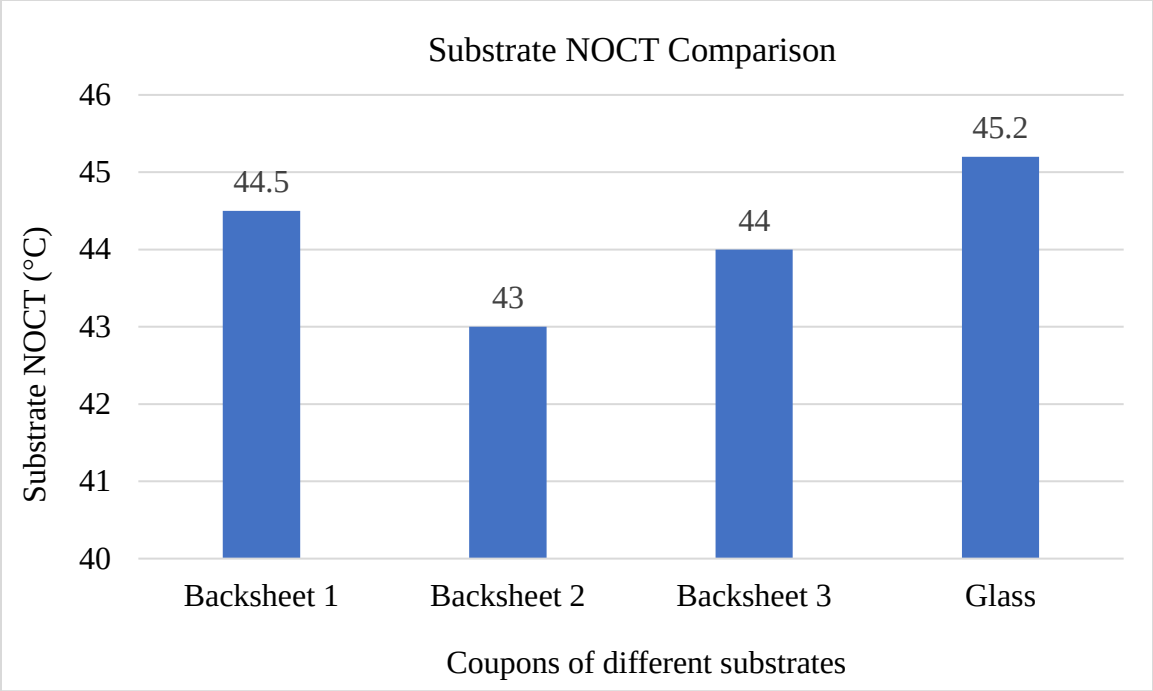

Figure 41 NOCT Comparison - Substrate Temperature

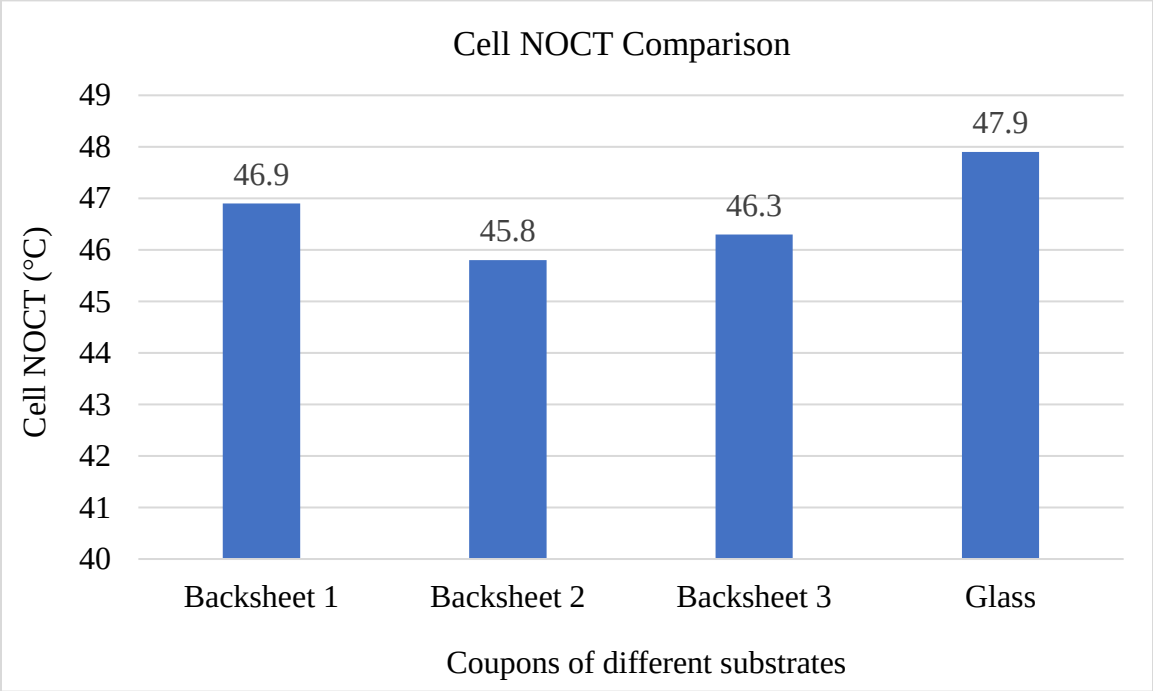

Figure 42 NOCT Comparison - Cell Temperature

4.5 Operating Temperature Comparison among Backsheet Substrate Coupons

In the previous section, the operating temperatures of all coupons based on NOCT weather condition were compared. Since the operating temperature based on NOCT is not the optimal way to demonstrate the advantage of thermally conductive backsheets, day to day operating temperature difference between hottest and coolest backsheet substrate coupon is presented. In the plot, >400 W/m^2 irradiance, >0.25 m/s windspeed and 9 AM to 3 PM data during the days of May 1-31, 2017 (excluding May 8, 2017), June 9 - July 30, 2017 (excluding June 12) was used. In the Figures 43 and 44 the operating temperature of the coolest coupon with backsheet type 2 substrate was compared with hottest backsheet substrate coupon of backsheet type 1.

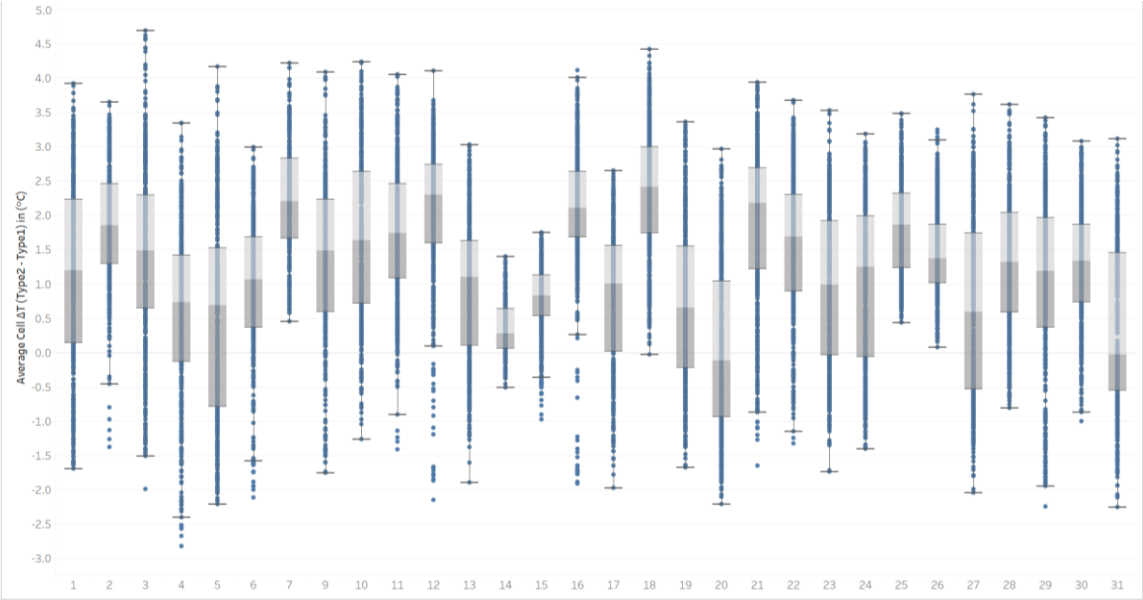

Figure 43 Averaged daily substrate temperature difference between coupons with backsheet substrates of different thermal conductivities (May 2017)

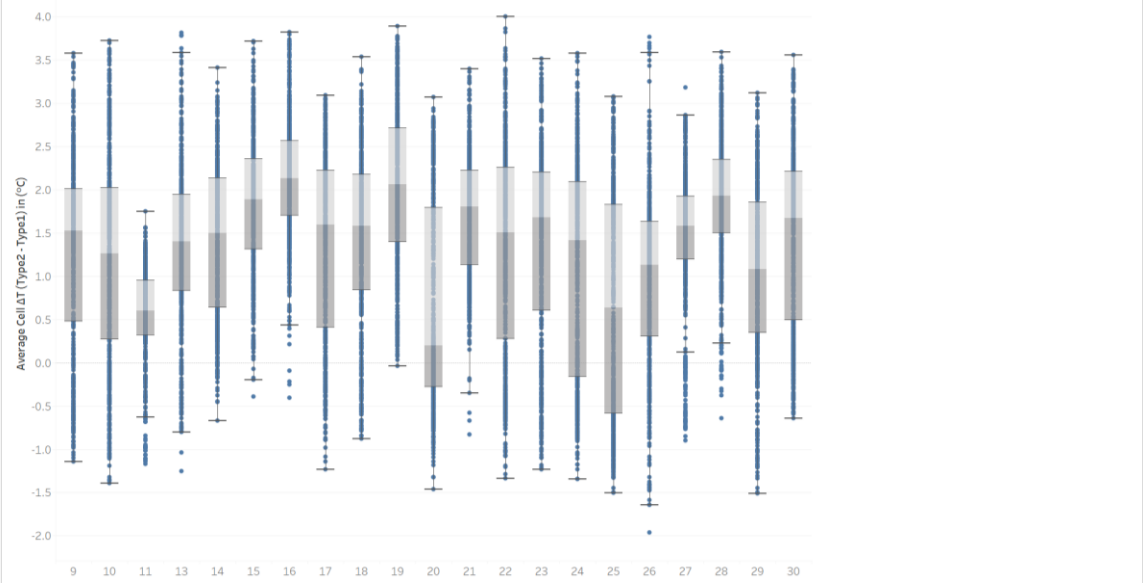

Figure 44 Averaged daily substrate temperature difference between coupons with backsheet substrates of different thermal conductivities (June 2017)

It can be seen that the even though temperature difference between the coupons of different backsheet substrates goes as high as 6-7 °C, the median value is more than 2 °C for most part of the May and June months. This can be attributed to higher axial thermal conductivity of type 2 backsheet than type 1 backsheet.

4.6 $\Delta T = (T_{cell} - T_{mod})$ Measurements

The ΔT measurements were performed for both backsheet and glass substrate coupons from the field data. The data from May 1-31, 2017 (excluding May 8, 2017), June 9 - July 12, 2017 (excluding June 12, July 5, July 11) were considered for analyzing the backsheet substrate coupons while the data from June 9 - July 12, 2017 (excluding June 12, July 5, July 11) were considered for analyzing the glass substrate coupons. The mean and standard deviation values of ΔT for backsheet substrate coupons are shown in the Table 12

Table 12 ΔT = (Tcell – Tmod) measurements

Substrate type	Mean ΔT	Standard deviation in ΔT
Backsheet type 1	1.72	1.42
Backsheet type 2	1.58	1.31
Backsheet type 3	1.59	1.39
Glass	1.61	1.21

For better visualization, day to day box plots of ΔT measurements for type 1 polymer backsheet and glass substrate coupons for each month are shown in the figure below. Since the day to day ΔT of backsheet type 2 and type 3 coupons were similar to coupon of backsheet type 1, they are not presented here. Even though the temperature difference goes up to 7 °C the median value remains around 1.5 °C to 2 °C for most of the days irrespective of the substrate type during the summer months. The figure 45 shows the box plots of day to day ΔT measurements for type 1 polymer backsheet for the date range considered.

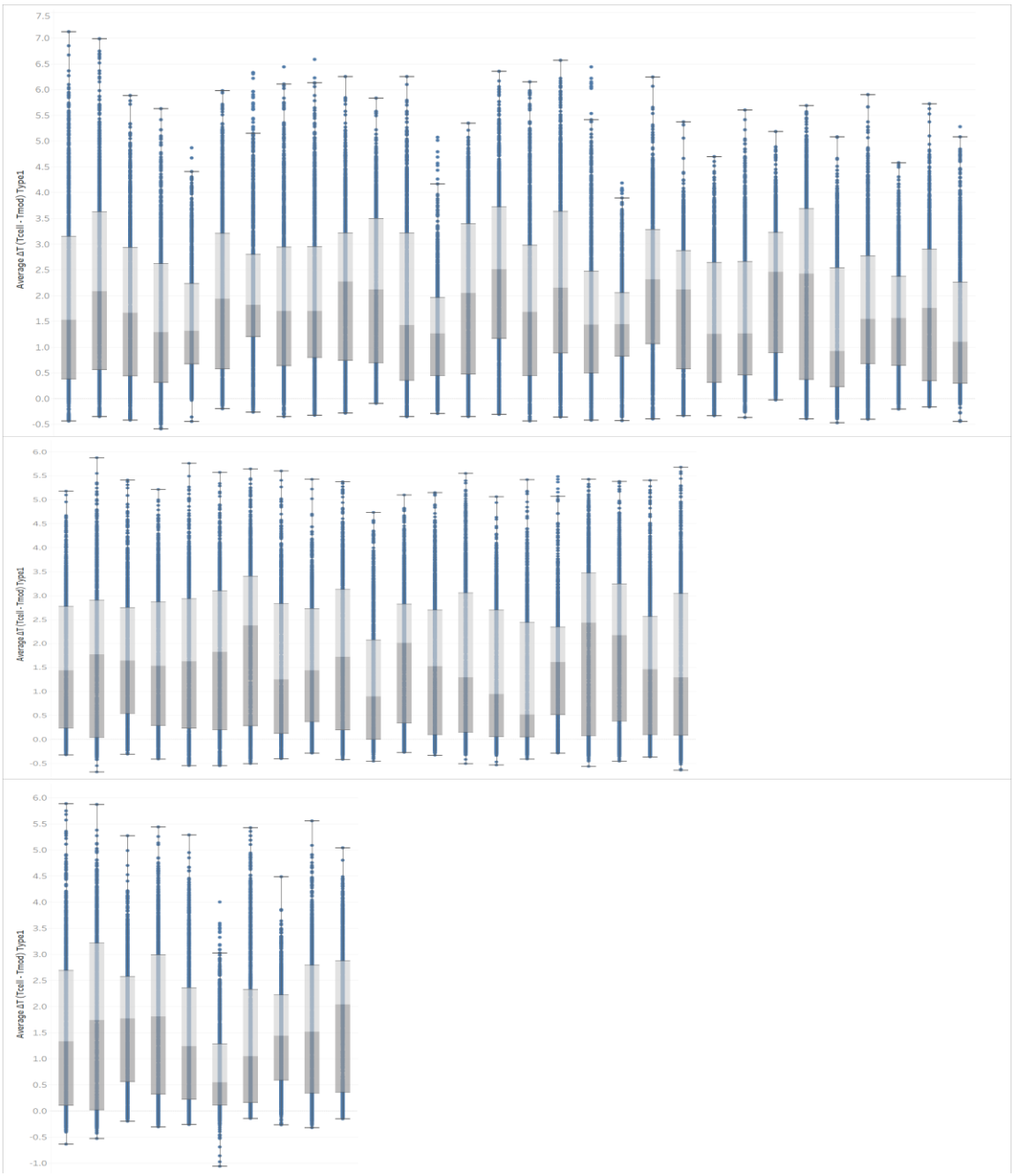

Figure 45 Day to day box plots of temperature difference (Tcell - Tmod) for coupons of type 1 backsheet substrate in the date range considered

The Figure 46 shows the box plots of day to day average ΔT measurements for glass coupons for the date range considered. It can be seen that the temperature difference ΔT show similar variation as that of the polymer backsheet substrate coupons.

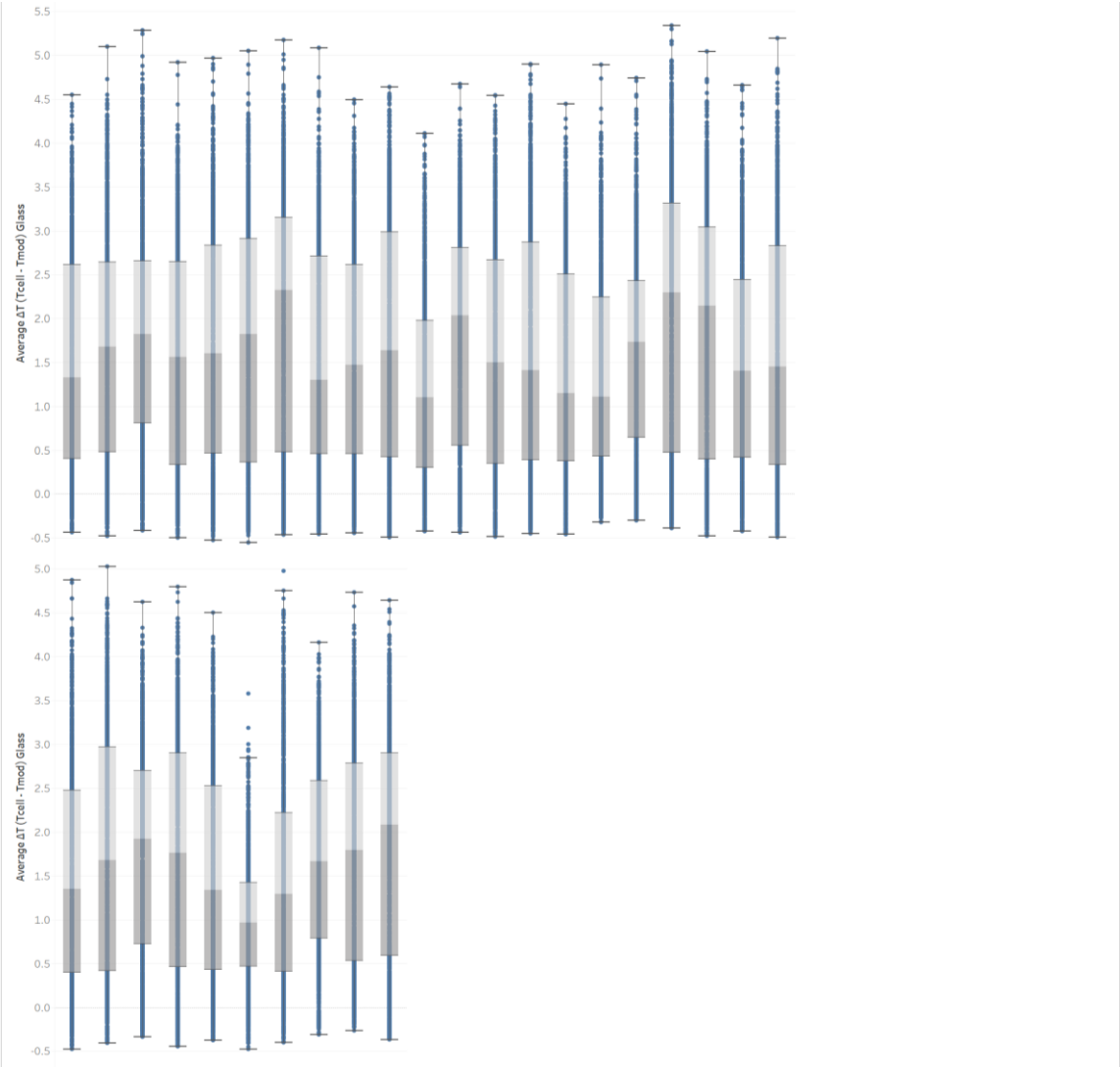

Figure 46 Day to day box plots of temperature difference (Tcell - Tmod) for coupons of glass substrate in the date range considered

The figures 47 and 48 show the average daylong time series plots from 7AM to 6 PM of temperature difference ΔT, irradiance, ambient temperature and windspeed for all the

coupons in the date range considered. It can be seen that ΔT data follows normal distribution and peaks around the noon time at about 3 °C irrespective of the substrate type.

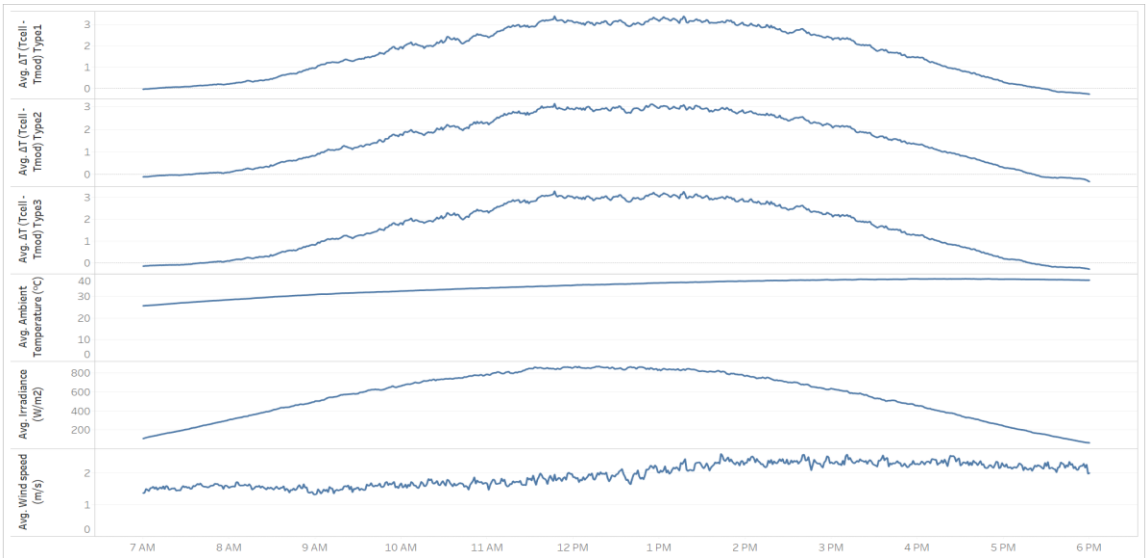

Figure 47 Daylong average time series plot of temperature difference of all backsheet substrate coupons along with ambient conditions

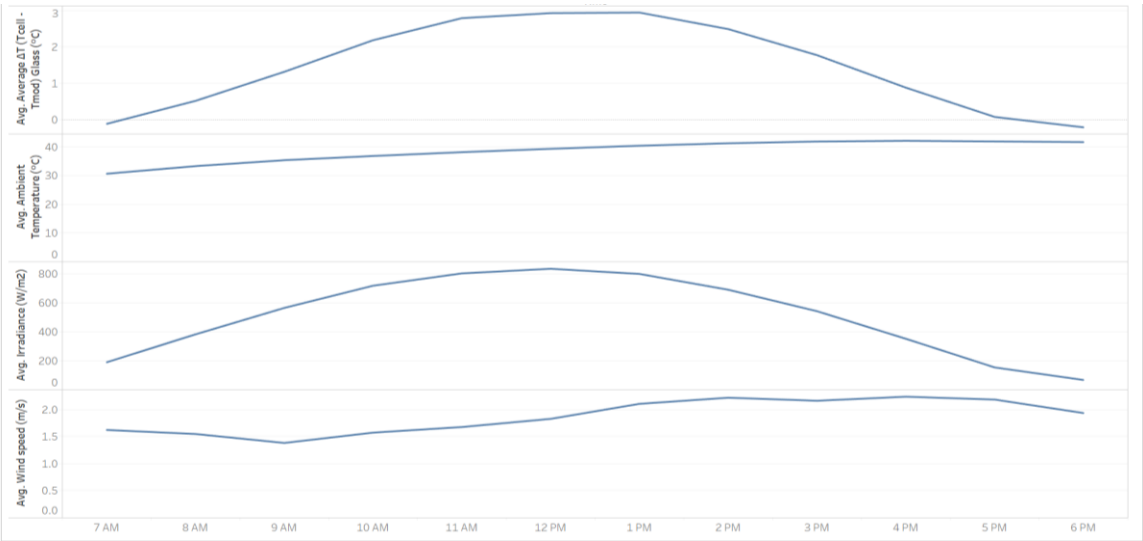

Figure 48 Daylong average time series plot of temperature difference of all glass substrate coupons along with ambient conditions

5. CONCLUSION

5.1 Thermal Model

Thermal modeling is an absolute necessity to understand the thermal performance of modules at varying ambient conditions. A simple linear relationship between module temperature and the ambient conditions has been derived using linear regression fit method. Similar prediction models have been derived for cell operating temperatures as well. In addition to ambient conditions dependence modeling, the effect of material properties on module and cell operating temperatures have also been modeled. It can be concluded that for glass-polymer modules, ambient temperature dictates the module and cell temperatures while irradiance and wind speed also contribute significantly. The thermal conductivity of the backsheet, wind direction and relative humidity also have a small impact on the module temperature and the model provides the necessary guidelines to module and backsheet manufacturers in the case of backsheet selection and design for improved passive cooling of the module. For glass-glass modules, irradiance and ambient temperature play the most significant role while wind speed also has some significance. The role of relative humidity is negligibly small in glass-glass modules than in glass-substrate modules.

5.2 NOCT and Operating Temperature - Effect of Thermal Conductivity of the Substrate

The nominal operating temperature based on both cell and module temperature was calculated for all coupons of each substrate type. It can be seen that there is a difference of around 1.5 °C in average NOCT value between coupons with backsheets of varying thermal conductivities. NOCT of the glass-glass coupons is at least 1 °C higher than all other glass-polymer coupons. It can be concluded that glass-polymer coupons operate at a

lower temperature in general and using backsheets of high heat dissipation capacity reduces the operating temperature which in turn reflects positively on the voltage. Since NOCT gives a single average value, day to day operating temperature of coupons with different backsheet substrates were compared and it can be concluded that coupon with highly thermally conductive backsheet operates about 2 °C cooler than coupon with lesser thermal conductivity for most part of the summer.

5.3 $\Delta T = (T_{cell} - T_{mod})$ Measurements

The $\Delta T = T_{cell} - T_{mod}$ measurements for the coupons irrespective of the substrate type has a mean value around 1.5 °C to 2 °C with a standard deviation of 1 °C to 1.5 °C. Hourly average for all days considered indicates that the temperature difference peaks around 3 °C during noon and follows normal distribution.

REFERENCES

[1] E. Skoplaki and J. A. Palyvos, “On the temperature dependence of photovoltaic module electrical performance: A review of efficiency/power correlations,” *Sol. Energy*, vol. 83, no. 5, pp. 614–624, 2009.

[2] E. L. Meyer and E. E. Van Dyk, “Assessing the reliability and degradation of photovoltaic module performance parameters,” *IEEE Trans. Reliab.*, vol. 53, no. 1, pp. 83–92, 2004.

[3] “http://www.pveducation.org/pvcdrom/effect-of-temperature - downloaded on June 2017.” .

[4] J. A. del Cueto, “Comparison of energy production and performance from flat-plate photovoltaic module technologies deployed at fixed tilt,” *Conf. Rec. Twenty-Ninth IEEE Photovolt. Spec. Conf. 2002.*, no. May, pp. 1523–1526, 2002.

[5] M. Green, *Operating principles, Technology and System Applications*. Prentice Hall, Inc, 1982.

[6] “Design qualification Type approval of commercial PV Modules, IEC 61215 10.6 Performance at NOCT with IEC 60904-3 reference solar spectral irradiance distribution,” 2005.

[7] “IEC 61853. Draft Performance Testing and Energy Rating of Terrestrial Photovoltaic.”

[8] Y. Tang, “Outdoor Energy Rating Measurements of Photovoltaic Modules,” Arizona State University, 2005.

[9] “International Electrotechnical Commission (IEC) standard, IEC 61215,” 2005.

[10] G. Tamizhmani, K. Paghasian, J. Kuitche, M. G. Vemula, and G. Sivasubramanian, “Photovoltaic Module Power Rating per IEC 61853-1 Standard : Solar America Board for Codes and Standards,” *Sol. Am. Board Codes Stand. Rep.*, p. 51, 2011.

[11] J. Kuitche *et al.*, “One year NOCT round-robin testing per IEC 61215 standard,” *Conf. Rec. IEEE Photovolt. Spec. Conf.*, pp. 002380–002385, 2011.

[12] “https://www.enfsolar.com/pv/backsheet - downloaded on June 2017.” .